Exact mean exit time for surface-mediated diffusion

J.-F. Rupprecht,[1] O. Bénichou,[1] D. S. Grebenkov,[2] and R. Voituriez[1]

[1]*Laboratoire de Physique Théorique de la Matière Condensée (UMR 7600), case courrier 121, Université Paris 6, 4 Place Jussieu, 75255 Paris Cedex*

[2]*Laboratoire de Physique de la Matière Condensée (UMR 7643), CNRS – Ecole Polytechnique, F-91128 Palaiseau Cedex France*

(Dated: November 16, 2012)

We present an exact expression for the mean exit time through the cap of a confining sphere for particles alternating phases of surface and of bulk diffusion. The present approach is based on an integral equation which can be solved analytically. In contrast to the statement of Berezhkovskii and Barzykin [J. Chem. Phys. **136**, 54115 (2012)], we show that the mean exit time can be optimized with respect to the desorption rate, under analytically determined criteria.

I. INTRODUCTION

Surface-mediated processes, in which a particle randomly alternates between surface and bulk diffusions, are relevant for various chemical and biochemical processes such as reactions in porous media or trafficking in living cells [1–10]. Recently, it has been shown theoretically that intermittent dynamics between two diffusive phases can lead to faster kinetics. The kinetics was characterized by the mean first passage time (MFPT) of diffusing particles to a fixed reactant [11].

As a representative example of confined interfacial kinetics, the case of a particle alternating bulk and surface diffusion over a sphere which contains a reactive cap, was considered in [12–14]. The reactive cap can also be interpreted as a hole, in which case the MFPT is referred to as the mean exit time [15–18]. While the desorption rate from the surface is independent of any geometrical parameter, the switching dynamics from the bulk to the surface is determined by the statistics of returns to the sphere. These statistics strongly depend on the boundary behavior of the process. After each desorption event, it was assumed in [12, 13] that the particle was ejected into the bulk at a distance $a > 0$ that was required to avoid an immediate re-adsorption on the perfectly adsorbing sphere. A similar description was used in discrete square lattice versions of this model, in which the lattice spacing played the role of the cut-off distance a [19, 20]. In these studies, the MFPT was found, under certain conditions, to be an optimizable function of the desorption rate. The favorable effect of desorptions was attributed in [12] to the fact that bulk excursions reduce the time wasted due to the recurrence of surface Brownian motion, by bringing particles through the bulk to unvisited regions of the sphere. Previous mean-field treatments which ignored spatial correlations, missed this possible optimum [21]. In the case of a uniformly semi-reflecting sphere, *including the target*, the MFPT was also found to be an optimizable function of the desorption rate even for a distance of ejection a set to zero [22].

Recently, a coarse-grained approach to the surface-mediated search for a perfectly adsorbing target in an otherwise semi-reflecting sphere was considered in [23]. This model is relevant in numerous real situations in which the particle reactivity with the target is not related to its affinity with the rest of the surface, as it is obviously the case in particular for exit problems. Relying on an elegant first order kinetics scheme, concise approximate expressions were proposed in [23] for the spatially averaged MFPTs (called here global MFPTs and denoted GMFPTs) for a uniform distribution of starting points over either the sphere surface or the bulk. These averages will be called hereafter surface and bulk GMFPTs. This approach, which treats the bulk and surface diffusive phases as two effective states coupled by first order kinetic equations, led to a monotonic GMFPT as a function of the desorption rate. This striking difference with Ref. [12] was attributed in [23] to the non-locality of the desorption process, in which the instantaneous ejection at a non zero distance a implied a violation of the detailed balance condition.

In this article we clarify this puzzling situation and address the question of the optimality of the GMFPTs as a function of the desorption rate for the mixed boundary condition of [23]. More precisely, (i) we provide an exact solution for the MFPT; (ii) we prove that the surface GMFPT can still be optimized with respect to the desorption rate, under analytically determined criteria; (iii) we compare our results with the coarse-grained approach of [23], which is shown to be accurate only in a limited region of the parameter space.

II. THE MODEL

We consider particles diffusing in a three-dimensional spherical cavity of radius R (see Fig. 1) switching between phases of surface diffusion with diffusion coefficient D_1 and phases of bulk diffusion with diffusion coefficient D_2. The time spent on the surface is assumed to follow an exponential law with desorption rate λ.

The target is a cap defined as the portion of the sphere $\theta \in [0, \epsilon]$, where θ is the elevation angle in spherical coordinates. The target is considered as perfectly reactive, i.e. particles react as soon as they encounter the target for the first time. We will focus here on the mean

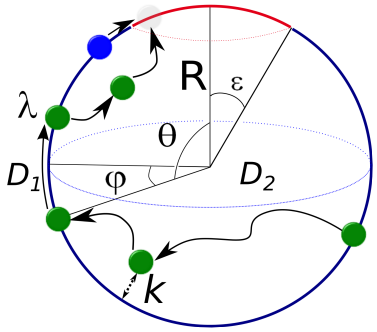

FIG. 1: (Color online). Model of surface-mediated diffusion in a sphere of radius R containing a perfectly adsorbing cap (a target). For finite values of k, particles (represented as small spheres) diffusing in the bulk randomly bind to or bounce from the remaining (non-adsorbing) part of the sphere surface (outside the target cap). The target is reached either from the bulk (shown by the green particle), or from the surface (shown by the blue particle).

first passage time (MFPT) on the target. The surface GMFPT $\langle t_1 \rangle$ is defined here as the average of the MFPT over a uniform distribution of the starting points on the sphere surface, *including the target*. In turn, in Ref. [23], the MFPT was averaged over the starting points outside the target; we denote this average as $\langle t_1 \rangle_{[1]}$. The two averages are related by $\langle t_1 \rangle = A \langle t_1 \rangle_{[1]}$, where A is a geometrical factor which is written as

$$A = \frac{1}{1 + \tan^2(\epsilon/2)}. \tag{1}$$

The non-reactive part of the sphere is considered as semi-reflecting: a particle reaching by bulk diffusion the non-reactive part of the sphere surface gets randomly either adsorbed or reflected back in the bulk. The probability for binding to the surface is an increasing function of the adsorption coefficient k, which will be precisely defined through the radiative boundary condition for the MFPT in Eq. (15). In particular, $k = \infty$ (resp. $k = 0$) corresponds to a perfectly adsorbing (resp. reflecting) boundary. Notice that the model that we consider here is exactly the same as in [23].

The limits $\lambda = 0$ and $\lambda = \infty$ correspond to simple situations. In the case $\lambda = 0$, particles are trapped on the surface until they reach the target, and the exact expression for the surface GMFPT is [26]:

$$t_s = \langle t_1 \rangle_{\lambda=0} = \frac{R^2}{D_1} \left(\ln \left(\frac{2}{1 - \cos\epsilon} \right) - \frac{1 + \cos\epsilon}{2} \right). \tag{2}$$

The limit $\lambda = \infty$ is equivalent to a purely reflecting boundary. The asymptotic behavior for the narrow escape limit $\epsilon \ll 1$ is given in [24]:

$$t_b = \langle t_1 \rangle_{\lambda=\infty} = \frac{\pi R^2}{3 D_2 \epsilon} \Big(1 + \epsilon \ln(\epsilon) + O(\epsilon) \Big). \tag{3}$$

Notice that the bulk and surface GMFPTs diverge as ϵ tends to zero, as it can be seen in particular in the above limits. Indeed a point-like target ($\epsilon = 0$) is detectable neither by bulk (3D) excursions nor by surface (2D) diffusion.

III. EXACT SOLUTION

A. Basic equations

Using a standard formalism of backward equations [27], we derive the diffusive equations (12,13) and the appropriate boundary conditions (14,15) satisfied by the MFPT, which we proceed to solve in the next section.

We define $p((r,\theta,\phi), s|(\boldsymbol{x'}, \phi'), t')$ (resp. $p((\theta,\phi), s|\boldsymbol{x'}, t')$) as the probability for a particle located at time t' at $\boldsymbol{x'}$ – with either $\boldsymbol{x'} = r', \theta'$ into the bulk or $\boldsymbol{x'} = \theta'$ on the sphere – to reach at time $s > t'$ the point (r,θ,ϕ) in the bulk (resp. the point (θ,ϕ) on the surface). In what follows, we omit the azimuthal coordinates by referring to probabilities averaged over the initial and final azimuthal angles:

$$p((r,\theta), s|\boldsymbol{x'}, t') \equiv \int_0^{2\pi} d\phi \int_0^{2\pi} d\phi' p((r,\theta,\phi), s|(\boldsymbol{x'}, \phi'), t').$$

For convenience, in this section we will use the shorthand notations

$$p((r,\theta), s|\boldsymbol{x'}, t') \equiv p(r,\theta), \qquad p(\theta, s|\boldsymbol{x'}, t') \equiv p(\theta). \tag{4}$$

Conversely, we define the conditional probabilities: $p(\bar{\boldsymbol{x}}, \bar{t}|(r,\theta), s) \equiv \bar{p}(r,\theta)$ and $p(\bar{\boldsymbol{x}}, \bar{t}|\theta, s) \equiv \bar{p}(\theta)$, with $\bar{t} > s$ and $\bar{x} = (\bar{r}, \bar{\theta})$ in the bulk or $\bar{x} = \bar{\theta}$ on the sphere.

In the following, the Laplace operator is $\Delta_{(r,\theta)} = \Delta_r + \Delta_\theta / r^2$ where Δ_r and Δ_θ are

$$\Delta_r = \frac{\partial^2}{\partial r^2} + \frac{2}{r} \frac{\partial}{\partial r}, \qquad \Delta_\theta = \frac{1}{\sin\theta} \, \partial_\theta \, (\sin\theta \, \partial_\theta). \tag{5}$$

1. *Diffusion equations*

For the process under study the conditional probability $p(r,\theta)$ satisfies the *forward* diffusion equations, for all $s > t'$, [23],

$$\frac{\partial p(r,\theta)}{\partial s} = D_2 \, \Delta_{(r,\theta)} \, p(r,\theta) \tag{6}$$

$$\frac{\partial p(\theta)}{\partial s} = \frac{D_1}{R^2} \Delta_\theta p(\theta) - \lambda \, p(\theta) + k D_2 \, p(R,\theta). \tag{7}$$

Each term in the right-hand side of Eq. (7) has a straightforward physical interpretation ; these are (from left to right) (i) the diffusion within the surface state; (ii) desorption events with a constant rate λ; (iii) adsorption events with a success rate quantified by k ([22]).

Equivalently to Eqs. (6) and (7), the conditional probabilities satisfy the backward equations, for all $t > s'$, [27]

$$\frac{\partial \bar{p}(r,\theta)}{\partial s} = -D_2\ \Delta_{(r,\theta)}\ \bar{p}(r,\theta). \tag{8}$$

$$\frac{\partial \bar{p}(\theta)}{\partial s} = -\frac{D_1}{R^2}\Delta_\theta\ \bar{p}(\theta) + \lambda\Big\{\bar{p}(\theta) - \bar{p}(R,\theta)\Big\} \tag{9}$$

These backward diffusion equations are commonly used to determine first passage time observables [28].

We define $t_1(\theta)$ as the MFPT for particles started on the sphere at the angle θ, and $t_2(r,\theta)$ stands for the MFPT for particles started at the bulk point (r,θ) (the second angular coordinate ϕ is irrelevant due to the symmetry and thus ignored). The MFPTs are expressed in terms of the conditional probabilities through the relations [27]

$$t_1(\theta) \equiv \int_0^\infty dt \left(\int_0^\pi 2\pi R^2 \sin\tilde{\theta} d\tilde{\theta}\ p(\tilde{\theta}, t|\theta, 0) + \int_{\mathcal{S}} 2\pi r^2 dr \sin\tilde{\theta} d\tilde{\theta}\ p(r,\tilde{\theta}, t|\theta, 0) \right), \tag{10}$$

$$t_2(r,\theta) \equiv \int_0^\infty dt \left(\int_0^\pi 2\pi R^2 \sin\tilde{\theta} d\tilde{\theta}\ p(\tilde{\theta}, t|r, \theta, 0) + \int_{\mathcal{S}} 2\pi r^2 dr \sin\tilde{\theta} d\tilde{\theta}\ p(r,\tilde{\theta}, t|r, \theta, 0) \right), \tag{11}$$

where $\mathcal{S} \equiv (0,R) \times (0, 2\pi)$.

Substituting the latter relations (10) and (11) into Eqs. (8,9), one can show that the MFPTs satisfy the set of equations

$$\frac{D_1}{R^2}\Delta_\theta t_1(\theta) + \lambda\left(t_2(R,\theta) - t_1(\theta)\right) = -1 \quad (\epsilon < \theta < \pi), \tag{12}$$

$$D_2\left(\Delta_r + \frac{\Delta_\theta}{r^2}\right)\ t_2(r,\theta) = -1 \quad ((r,\theta) \in \mathcal{S}). \tag{13}$$

In the next section we specify the appropriate boundary conditions for the MFPT.

2. Boundary conditions

We justify that the B.C. for the process defined in Sec. II are:

(i) the Dirichlet boundary condition

$$t_1(\theta) = 0 \qquad (0 \le \theta \le \epsilon), \tag{14}$$

which expresses that the search process is stopped on the target.

(ii) the mixed boundary condition

$$t_2(R,\theta) = \begin{cases} 0 & (0 \le \theta \le \epsilon), \\ t_1(\theta) - \dfrac{1}{k}\dfrac{\partial t_2}{\partial r}_{|\mathbf{r}=(R,\theta)} & (\epsilon < \theta \le \pi), \end{cases} \tag{15}$$

in which the first relation expresses perfect adsorption on the target ($\theta \in [0,\epsilon]$) while the second relation (radiative B.C.) implements an imperfect adsorption process on the rest of the surface ($\theta \in [\epsilon, \pi]$). The mixed boundary condition (15) is the major difference of the present model from the previously studied case [22], in which the radiative B.C. was imposed over the whole boundary, including the target. Although this modification may seem minor, the difference on the target reactivity has a drastic effect on the surface GMFPT for short adsorption times ($\lambda \gg D_1/R^2$) or low adsorption rates ($kR \ll 1$), as shown in Fig. 6 below.

In order to justify the form of the radiative B.C. (15), we determine the backward B.C. on the probability distribution from a well-known forward B.C. For the process defined in Sec. II, the forward B.C. equation on the probability distribution is [23]

$$D_2\frac{\partial p(r,\theta)}{\partial r}_{|r=R} = -\ kD_2\ p(R,\theta) + \lambda p(\theta). \tag{16}$$

Since the stochastic process under study is Markovian, one obtains the following Chapman-Kolmogorov equation on the conditional probabilities, for $\bar{t} > s > t'$,

$$p(\bar{\boldsymbol{x}}, \bar{t}|\boldsymbol{x}', t') = \int_0^\pi \int_0^R 2\pi r^2 dr \sin\theta d\theta\ \bar{p}(r,\theta) p(r,\theta) + \int_0^\pi 2R^2\pi \sin\theta d\theta\ \bar{p}(\theta) p(\theta). \tag{17}$$

Taking the derivative with respect to the intermediate time s of the above relation leads to the identity

$$\int_0^\pi \int_0^R 2\pi r^2 \sin\theta d\theta dr \left(\frac{\partial p(r,\theta)}{\partial s}\bar{p}(r,\theta) + p(r,\theta)\frac{\partial \bar{p}(r,\theta)}{\partial s}\right) + \int_0^\pi 2\pi R^2 \sin\theta d\theta \left(\frac{\partial p(\theta)}{\partial s}\bar{p}(\theta) + \frac{\partial \bar{p}(\theta)}{\partial s} p(\theta)\right) = 0.$$

The next step is to substitute diffusion Eqs. (6 – 8) into the last relation. The two terms with the angular Laplace operators cancel each other due to its hermiticity:

$$\int_0^\pi \sin\theta d\theta \left(\Delta_\theta\ \bar{p}(\theta) p(\theta) - \Delta_\theta\ p(\theta)\bar{p}(\theta)\right) = 0.$$

The divergence theorem applied on the bulk Laplacian $\Delta_{(r,\theta)}$ and the backward equations (8,9) yield the following relation over the sphere surface:

$$0 = \int_0^\pi 2R^2\pi \sin\theta d\theta \Big(D_2\frac{\partial p(r,\theta)}{\partial r}_{|R}\bar{p}(r,\theta) - D_2\frac{\partial \bar{p}(r,\theta)}{\partial r}_{|R} p(r,\theta) + \lambda\Big\{\bar{p}(\theta) - \bar{p}(R,\theta)\Big\} p(\theta) + \Big\{-\lambda\ p(\theta) + kD_2\ p(R,\theta)\Big\}\bar{p}(\theta)\Big),$$

which is satisfied only if:

$$D_2\frac{\partial \bar{p}(r,\theta)}{\partial r}_{|R}\ p(R,\theta) = D_2\frac{\partial p(r,\theta)}{\partial r}_{|R}\bar{p}(R,\theta) - \lambda\ \bar{p}(R,\theta) p(\theta) + kD_2\ p(R,\theta)\bar{p}(\theta). \tag{18}$$

Insertion of the forward B.C. (16) into Eq. (18) gives the B.C. on the backward probability distribution

$$\frac{\partial p(\bar{\boldsymbol{x}},\bar{t}|(r,\theta),s)}{\partial r}_{|r=R} = k\big\{p(\bar{\boldsymbol{x}},\bar{t}|\theta,s) - p(\bar{\boldsymbol{x}},\bar{t}|(r,\theta),s)\big\}_{|R}. \tag{19}$$

We then integrate Eq. (19) over the space and time variables $\boldsymbol{x}$ and t according to Eqs. (10) and (11) to obtain the B.C. on the MFPT:

$$\frac{\partial t_2}{\partial r}_{|\mathbf{r}=(R,\theta)} = k\big\{t_1(\theta) - t_2(R,\theta)\big\} \qquad (\epsilon \le \theta \le \pi),$$

which identifies with Eq. (15). Agreement with the B.C. used in [22] is discussed in Appendix A.

B. Integral equation

From the set of Eqs. (12) - (15) we now derive an integral equation on t_1 only.

We first recall that the eigenfunctions of the angular Laplace operator Δ_θ of Eq. (5) are expressed in terms of the Legendre polynomials P_n:

$$-\Delta_\theta P_n(\cos\theta) = \rho_n P_n(\cos\theta) \quad (n \ge 0), \tag{20}$$

where $\rho_n = n(n+1)$. We set $V_n(\theta) = \sqrt{2n+1}P_n(\cos\theta)$ to get the orthonormality: $\langle V_n|V_m\rangle = \delta_{nm}$, where the inner product is defined as

$$(f,g) \to \langle f|g\rangle_\epsilon \equiv \frac{1}{2}\int_\epsilon^\pi f(\theta)g(\theta)\sin\theta d\theta, \tag{21}$$

and $\langle f|g\rangle$ is the scalar product for $\epsilon = 0$. We also define

$$K^{(\epsilon)}_{mn} \equiv \langle V_n|V_m\rangle_\epsilon \qquad (m,n \ge 0), \tag{22}$$

with the explicit expressions listed in Table I.

The starting point for solution of the set of equations (12 and (13) is a Fourier decomposition of $t_2(r,\theta)$,

$$t_2(r,\theta) = \alpha_0 - \frac{r^2}{2dD_2} + \sum_{n=1}^\infty \alpha_n \left(\frac{r}{R}\right)^n V_n(\theta), \tag{23}$$

where $d = 3$ for the three-dimensional spherical cavity considered here (in Appendix E, we show how this approach can be directly translated for two-dimensional problems).

Due to the B.C. (15), the projection of $t_2(R,\theta)$ onto the orthonormal basis $\{V_n(\theta)\}_{n\ge0}$, is

$$\int_0^\pi t_2(R,\theta)V_n(\theta)\sin\theta d\theta = \int_\epsilon^\pi t_1(\theta)V_n(\theta)\sin\theta d\theta - \int_\epsilon^\pi \frac{1}{k}\frac{\partial t_2}{\partial r}_{|R} V_n(\theta)\sin\theta d\theta. \tag{24}$$

$V_n(\theta)$	$\sqrt{2n+1}\ P_n(\cos\theta)$
u	$\cos\epsilon$
$F_n(u), n \ge 1$	$\sum_{k=1}^n 2(u-1)P_k^2(u) + [P_k(u) - P_{k-1}(u)]^2$ $-(u-1)P_n^2(u) + (u-1)P_0^2(u) + u$
$g_\epsilon(\theta)$	$\ln\left(\frac{1-\cos(\theta)}{1-\cos(\epsilon)}\right)$
$\langle g_\epsilon\|1\rangle_\epsilon \equiv \langle g_\epsilon\rangle_\epsilon$	$\ln\left(\frac{2}{1-\cos\epsilon}\right) - \frac{1+\cos\epsilon}{2}$
$\xi_n\ (n \ge 1)$	$-\frac{\sqrt{2n+1}}{2}\left(\left(1+\frac{nu}{n+1}\right)P_n(u) + \frac{P_{n-1}(u)}{n+1}\right)$
$K^{(\epsilon)}_{00}$	$\frac{1+\cos(\epsilon)}{2}$
$K^{(\epsilon)}_{n0}\quad (n \ge 1)$	$\frac{P_{n+1}(u)-P_{n-1}(u)}{2\sqrt{2n+1}}$
$K^{(\epsilon)}_{nn}\quad (n \ge 1)$	$\frac{F_n(u)+1}{2}$
$K^{(\epsilon)}_{nm}\quad (m \ne n)$ $n,m \ge 1$	$\frac{\sqrt{2n+1}\sqrt{2m+1}}{2(m(m+1)-n(n+1))}\left((m-n)uP_m(u)P_n(u) + nP_{n-1}(u)P_m(u) - mP_{m-1}(u)P_n(u)\right)$
$I^{(\epsilon)}_{nn}\quad (n \ge 1)$	$\frac{2n+1}{2}\left(-P_n(u)\frac{uP_n(u)-P_{n-1}(u)}{n+1} + \frac{F_n(u)+1}{2n+1}\right)$
$I^{(\epsilon)}_{nm}\quad (m \ne n)$ $m,n \ge 1$	$\frac{\sqrt{2n+1}\sqrt{2m+1}m}{2(n+1)[m(m+1)-n(n+1)]}\left((n-m)uP_m(u)P_n(u) + (m+1)P_m(u)P_{n-1}(u) - (n+1)P_n(u)P_{m-1}(u)\right)$

TABLE I: Summary of the quantities involved in the computation of the vector $\boldsymbol{\xi}$ and the matrices Q and P in Eqs. (43) and (45) that determine the Fourier coefficients d_n of $t_1(\theta)$ according to Eq. (47).

The Fourier decomposition (23) leads to linear equations on the coefficients α_0 and α_n, $n \ge 1$,

$$\alpha_0 - \frac{R^2}{2dD_2}\left(1 + \frac{2K^{(\epsilon)}_{00}}{kR}\right) = \big\langle t_1\big|1\big\rangle - \sum_{m=1}^\infty \frac{mK^{(\epsilon)}_{0m}}{kR}\ \alpha_m, \tag{25}$$

$$\alpha_n + \sum_{m=1}^\infty \frac{mK^{(\epsilon)}_{nm}}{kR}\ \alpha_m = \big\langle t_1\big|V_n\big\rangle + \frac{RK^{(\epsilon)}_{n0}}{dkD_2}. \tag{26}$$

First, one can solve the set of linear equations (26), independently of Eq. (25), by writing

$$\sum_{m=1}^\infty (\delta_{n,m} + M_{nm})\,\alpha_m = \hat{U}_n, \tag{27}$$

where

$$M_{nm} \ \equiv\ \frac{m}{kR}K^{(\epsilon)}_{nm}, \tag{28}$$

$$\hat{U}_n \ \equiv\ \big\langle t_1\big|V_n\big\rangle + \frac{R}{dkD_2}K^{(\epsilon)}_{n0} \tag{29}$$

for all $n, m \ge 1$. Formally, the solution of this system of equations is

$$\alpha_n = \left[(\mathbb{I} + M)^{-1}\,\hat{U}\right]_n, \tag{30}$$

where $(\mathbb{I})_{n,m} = \delta_{n,m}$ stands for the identity matrix. Note that $t_1(\theta)$ and thus $\hat{U}_n$ are still unknown.

Second, substituting the B.C. (15) into the diffusion equation (12) leads to

$$-\frac{D_1}{R^2}\Delta_\theta t_1(\theta) = -1 + \frac{\lambda}{k}\frac{\partial t_2}{\partial r}_{|\mathbf{r}=(R,\theta)}. \quad (31)$$

The substitution of Eq. (23) into this relation yields

$$-\Delta_\theta t_1(\theta) = -\omega^2 T + \omega^2 \sum_{n=1}^{\infty} \alpha_n \frac{n}{kR} V_n(\theta), \quad (32)$$

where we defined

$$\omega \equiv R\sqrt{\lambda/D_1}, \quad (33)$$

$$T \equiv \frac{1}{\lambda} + \frac{1}{\alpha}, \quad (34)$$

α being the inverse of the mean re-adsorption time on the surface after a desorption event, as defined in [23]

$$\alpha \equiv \frac{dkD_2}{R}. \quad (35)$$

The solution of Eq. (32) which satisfies the B.C. $t_1(\epsilon) = 0$, is

$$t_1(\theta) = \omega^2 T g_\epsilon(\theta) - \omega^2 \sum_{n=1}^{\infty} \alpha_n \frac{n}{kR} \frac{V_n(\theta) - V_n(\epsilon)}{\rho_n} \quad (36)$$

for $\epsilon < \theta < \pi$, and $t_1(\theta) = 0$ otherwise ($0 \le \theta \le \epsilon$). Here, $R^2 g_\epsilon(\theta)/D_1$ is the well-known MFPT for a surface search (i.e. when $\lambda = 0$) [28]:

$$g_\epsilon(\theta) = \ln\left(\frac{1-\cos(\theta)}{1-\cos(\epsilon)}\right) \quad (37)$$

for $\epsilon < \theta < \pi$, and $g_\epsilon(\theta) = 0$ otherwise. One can easily check that $-\Delta_\theta g_\epsilon = -1$ and $g_\epsilon(\epsilon) = 0$. Using the formal expression (30) for α_n and introducing the dimensionless function

$$\psi(\theta) = \frac{t_1(\theta)}{\omega^2 T}, \quad (38)$$

one can represent Eq. (36) as an integral equation on $\psi(\theta)$:

$$\psi(\theta) = g_\epsilon(\theta) + \sum_{n,m=1}^{\infty} \frac{V_n(\theta) - V_n(\epsilon)}{\rho_n} X_{nm} \times\left(\frac{R}{dkD_2 T} K_{0m}^{(\epsilon)} + \omega^2 \langle \psi | V_m \rangle\right) \quad (39)$$

for $\epsilon < \theta < \pi$, and $\psi(\theta) = 0$ otherwise. Here, we introduced

$$X_{nm} \equiv -\frac{n}{kR}\left[(\mathbb{I} + M)^{-1}\right]_{nm}. \quad (40)$$

C. Exact solution

Expanding the function $\psi(\theta) - g_\epsilon(\theta)$ on the complete basis of functions $\{V_n(\theta) - V_n(\epsilon)\}_{n\ge 1}$,

$$\psi(\theta) = g_\epsilon(\theta) + \sum_{n=1}^{\infty} d_n \{V_n(\theta) - V_n(\epsilon)\} \quad (\epsilon < \theta < \pi), \quad (41)$$

one obtains a set of linear equations for the unknown coefficients $\{d_n\}_{n\ge 1}$

$$\sum_{n=1}^{\infty} d_n \{V_n(\theta) - V_n(\epsilon)\} = \omega^2 \sum_{n=1}^{\infty} \left(U_n + \sum_{l=1}^{\infty} Q_{nl} d_l\right) \{V_n(\theta) - V_n(\epsilon)\}, \quad (42)$$

where we defined the vectors $\boldsymbol{U}$ and $\boldsymbol{\xi}$ by their n-th coordinates ($n \ge 1$)

$$U_n \equiv \frac{1}{\rho_n} \sum_{m=1}^{\infty} X_{nm} \left(\frac{\xi_m}{\rho_m} + \frac{K_{0m}^{(\epsilon)} R}{dkD_2 \omega^2 T}\right), \quad (43)$$

$$\xi_n \equiv \rho_n \langle g_\epsilon | V_n \rangle_\epsilon, \quad (44)$$

and the matrices Q and $I^{(\epsilon)}$ by their n-th row and l-th column ($n, l \ge 1$)

$$Q_{nl} \equiv \frac{1}{\rho_n} \sum_{m=1}^{\infty} X_{nm}\, I_{ml}^{(\epsilon)}, \quad (45)$$

$$I_{ml}^{(\epsilon)} \equiv \langle V_m(\theta) | V_l(\theta) - V_l(\epsilon) \rangle_\epsilon. \quad (46)$$

As Eq. (42) is satisfied for all $\theta \in [\epsilon, \pi]$, the coefficients d_n are found as

$$d_n = \left[\omega^2 \left(\mathbb{I} - \omega^2 Q\right)^{-1} U\right]_n. \quad (47)$$

Combining this relation with Eqs. (37, 38, 41), one finally obtains an exact representation for the MFPT

$$t_1(\theta) = \omega^2 T \left(g_\epsilon(\theta) + \sum_{n=1}^{\infty} d_n \{V_n(\theta) - V_n(\epsilon)\}\right) \quad (48)$$

for $\epsilon < \theta \le \pi$, and $t_1(\theta) = 0$ for $0 \le \theta \le \epsilon$.

Averaging $t_1(\theta)$ over the whole surface and using the relation

$$\langle P_n(\cos\theta) - P_n(\cos\epsilon) | 1 \rangle_\epsilon = \rho_n \langle P_n(\cos\theta) | g_\epsilon(\theta) \rangle_\epsilon = \xi_n,$$

we obtain the exact formula for the surface GMFPT:

$$\langle t_1 \rangle = \omega^2 T \left(\langle g_\epsilon \rangle + \sum_{n=1}^{\infty} d_n \xi_n\right), \quad (49)$$

where $\langle g_\epsilon \rangle$ is computed by integrating Eq. (37):

$$\langle g_\epsilon \rangle = \ln\left(\frac{2}{1-\cos\epsilon}\right) + \frac{1+\cos\epsilon}{2}. \quad (50)$$

Equations (48) and (49) are among the main results of the paper, and several comments are in order:

(i) As expected, in both limits $\lambda = 0$ and $k = \infty$, we retrieve the limit of the MFPTs for the surface search process alone: $t_1(\theta) \to \frac{R^2}{D_1} g_\epsilon(\theta)$.

(ii) A physical interpretation of Eq. (49) is that the surface GMFPT is the product of the mean time $T = \lambda^{-1} + \alpha^{-1}$ for an elementary cycle composed of one surface exploration and one bulk excursion, by the mean number of cycles before reaching the target.

(iii) A numerical implementation of the exact solutions in Eqs. (48) and (49) requires a truncation of the infinite-dimensional matrix Q to a finite size $N \times N$. After a direct numerical inversion of the truncated matrices $(\mathbb{I} + M)$ in Eq. (30) and $(\mathbb{I} - \omega^2 Q)$ in Eq. (47), the MFPTs from Eqs. (48, 49) are approximated by truncated series (with N terms). At a fixed tolerance threshold, higher values of λ require higher values of N. In spite of the truncation, we will refer to the results obtained by this numerical procedure as *exact solutions*, as their accuracy can be arbitrarily improved by increasing the truncation size N.

(iv) The expression (49) is valid for arbitrary target size ϵ, provided that the series are truncated at sufficiently high N.

Substituting Eqs. (38) and (41) into Eq. (29), we deduce the Fourier coefficients α_n of $t_2(r,\theta)$ for $n \geq 1$

$$\alpha_n = \sum_{m=1}^{\infty} \left((\mathbb{I} + M)^{-1}\right)_{nm} \times \left(\omega^2 T \left[\frac{\xi_m}{\rho_m} + (I^{(\epsilon)}\boldsymbol{d})_m\right] + \frac{R K^{(\epsilon)}_{m0}}{dk D_2}\right), \tag{51}$$

while α_0 is found from Eq. (25). The coefficients α_n determine an exact representation (23) of the MFPT $t_2(r,\theta)$. Therefore one gets a complete exact solution of the problem for any starting point. In particular, the bulk GMFPT $\langle t_2 \rangle$ averaged over uniformly distributed starting points in the bulk, reads

$$\langle t_2 \rangle \equiv \frac{2\pi}{4\pi R^3/3} \int_0^R dr\, r^2 \int_0^\pi d\theta\, \sin\theta\, t_2(r,\theta) = \alpha_0 - \frac{3R^2}{10 d D_2}, \tag{52}$$

since the other terms from Eq. (23) vanish due to the orthogonality of $V_n(\theta)$. Substituting an expression for α_0, one gets

$$\langle t_2 \rangle = \langle t_1 \rangle + \frac{R^2}{2dD_2}\left(\frac{2}{5} + \frac{2K^{(\epsilon)}_{00}}{kR}\right) - \sum_{m,n=1}^{\infty} \frac{m K^{(\epsilon)}_{0m}}{kR} \alpha_m. \tag{53}$$

Note that the coefficients α_n in Ref. [22] were simply proportional to the coefficients d_n, up to the third order in ϵ. The mixed boundary condition (15) results in the more sophisticated expression (51) for α_n.

D. Existence of an optimum

Despite the prediction of [23] that the bulk and surface GMFPTs are monotonic functions of λ, the exact solutions prove to admit a minimum, as seen in Fig. 3b on the example of the surface GMFPT. In this section we focus on the surface GMFPT and we determine sufficient conditions for this GMFPT to be an optimizable function of λ, which are set by two requirements: (i) desorption events should decrease the search time for small enough values of λ, i.e. $\langle t_1 \rangle < \langle t_1 \rangle_{\lambda=0} = t_s$; (ii) the mean surface search time is lower than the mean bulk search time, i.e. $t_s < t_b$.

The first condition is fulfilled when the derivative of the surface GMFPT is negative at $\lambda = 0$. We first rewrite the coefficients U_n as

$$U_n = Z_n + \frac{1}{dkR + \lambda \frac{R^2}{D_2}} \frac{D_1}{D_2} W_n, \tag{54}$$

where

$$Z_n \equiv \frac{1}{\rho_n} \sum_{m=1}^{\infty} X_{nm}\, \frac{\xi_m}{\rho_m}, \tag{55}$$

$$W_n \equiv \frac{1}{\rho_n} \sum_{m=1}^{\infty} X_{nm}\, K^{(\epsilon)}_{0m}. \tag{56}$$

The derivative of the GMFPT at $\lambda = 0$ is

$$\left(\frac{\partial \langle t_1 \rangle}{\partial \lambda}\right)_{\lambda=0} = \frac{R^4}{D_1^2}\left(\frac{D_1}{dkRD_2}\Big(\langle g_\epsilon \rangle + (\boldsymbol{\xi}\cdot\boldsymbol{W})\Big) + (\boldsymbol{\xi}\cdot\boldsymbol{Z})\right). \tag{57}$$

This derivative is negative provided that

$$\frac{D_2}{D_1} \geq \left(\frac{D_2}{D_1}\right)_{\rm low}, \quad \left(\frac{D_2}{D_1}\right)_{\rm low} = -\frac{1}{dkR}\, \frac{\langle g_\epsilon \rangle + (\boldsymbol{\xi}\cdot\boldsymbol{W})}{(\boldsymbol{\xi}\cdot\boldsymbol{Z})}, \tag{58}$$

where we used the inequality $(\boldsymbol{\xi}\cdot\boldsymbol{Z}) < 0$.

The second bound (ii) is obtained when the surface search time $R^2\langle g_\epsilon \rangle / D_1$ (at zero desorption rate) is lower than the search time at infinite desorption rate. Using the first-order asymptotic expansion of Eqs. (2, 3), this condition is explicitly given up to the second order in $\epsilon \ll 1$ as

$$\frac{D_2}{D_1} \leq \left(\frac{D_2}{D_1}\right)_{\rm up}, \tag{59}$$

$$\left(\frac{D_2}{D_1}\right)_{\rm up} = \frac{\pi}{3\epsilon(1 - \epsilon\ln\epsilon)(2\ln(2/\epsilon) - 1)} + O(\epsilon).$$

Combining the above inequalities, one gets a sufficient condition for the surface GMFPT to be optimizable for $\epsilon \ll 1$:

$$\left(\frac{D_2}{D_1}\right)_{\rm low} \leq \frac{D_2}{D_1} \leq \left(\frac{D_2}{D_1}\right)_{\rm up}. \tag{60}$$

Figure 4 displays the regime of parameters for which the surface GMFPT is optimizable.

E. Perturbative solution

The first terms of a perturbative expansion with respect to ϵ of Eq. (49) can easily be obtained. At first order in ϵ, one has

$$U_n = U_n^{(0)} + O(\epsilon) = \frac{\sqrt{2n+1}}{n^2(n+1)^2} \frac{\frac{n}{kR}}{1+\frac{n}{kR}} + O(\epsilon),$$
$$Q_{mn} = Q_{mn}^{(0)} + O(\epsilon) = \frac{1}{n(n+1)} \frac{\frac{n}{kR}}{1+\frac{n}{kR}} \delta_{m,n} + O(\epsilon),$$

from which

$$d_n = \omega^2 \left[(\mathbb{I} - \omega^2 Q^{(0)})^{-1} U^{(0)} \right]_n + O(\epsilon)$$
$$= \frac{\omega^2}{n(n+1)} \frac{\left(\frac{\frac{n}{kR}}{1+\frac{n}{kR}}\right)(2n+1)}{n(n+1) + \omega^2 \left(\frac{n/kR}{1+n/kR}\right)} + O(\epsilon).$$

One finds therefore

$$\psi(\theta) = -2\ln\epsilon + 2\ln\left(2\sin(\theta/2)\right)$$
$$- \omega^2 \sum_{n=1}^{\infty} \left(\frac{\frac{n}{kR}}{1+\frac{n}{kR}}\right) \frac{2n+1}{n(n+1)} \frac{1 - P_n(\cos\theta)}{n(n+1) + \omega^2 \left(\frac{\frac{n}{kR}}{1+\frac{n}{kR}}\right)}$$
$$+ O(\epsilon). \quad (61)$$

Averaging the latter relation over θ yields:

$$\langle t_1 \rangle = \omega^2 T \Bigg(2\ln(2/\epsilon) - 1$$
$$- \omega^2 \sum_{n=1}^{\infty} \frac{2n+1}{n(n+1)} \frac{\frac{n}{kR}}{n(n+1)(1+\frac{n}{kR}) + \omega^2 \frac{n}{kR}} + O(\epsilon) \Bigg). \quad (62)$$

Notice that this expression is identical to the perturbative development at $\epsilon \ll 1$ for the case of a uniformly semi-reflecting sphere, *including the target* [22]. In the limit of very small ϵ, the target is mainly reached from the adsorbed (surface) state, while its reactivity from the bulk is expected to be negligible. As seen on Fig. 3, the smaller the desorption rate λ, the larger the domain of applicability in ϵ of the perturbative development. Note also that in Fig. 3b, the first-order expression exhibits a minimum with respect to the desorption rate.

IV. COMPARISON WITH THE COARSE-GRAINED METHOD

A. Coarse-grained approach

In the coarse-grained approach of [23], the bulk, the target and the rest of the surface are considered as effective states, denoted by b, s and $\varnothing$, with no inner spatial degrees of freedom. An effective set of kinetic equations combines four first-order reaction rates: (i) the rate λ (denoted as β in [23]) which is associated with the desorption ($s \to b$); (ii) the rate α defined in Eq. (35) as the inverse of the mean re-adsorption time on the sphere, which is associated with the effective adsorption ($b \to s$); (iii) the rate k_s defined as the inverse of the surface GMFPT of Eq. (2) for the surface search alone ($s \to \varnothing$):

$$k_s = \frac{A}{t_s}, \quad (63)$$

where the prefactor A from Eq. (1) accounts for the difference between the averages over the initial position mentioned above; (iv) the rate k_b defined as the inverse of the bulk GMFPT of Eq. (3) for the bulk search alone ($b \to \varnothing$). As in [23], we define

$$k_b \equiv \frac{dD_2\epsilon}{\pi R^2}, \quad (64)$$

which is the inverse of the first-order asymptotics in the limit $\epsilon \ll 1$ of Eq. (3).

In the following, we focus on the MFPT averaged over the sphere surface $\langle t_1 \rangle$ and compare our exact expression Eq. (49) to the concise approximate expression derived in [23] for the surface GMFPT

$$\langle t_1 \rangle \simeq A \frac{\alpha + \lambda + k_b}{\alpha k_s + \lambda k_b + k_b k_s}. \quad (65)$$

As found in [23], this expression predicts a monotonic behavior for the surface GMFPT as a function of the desorption rate λ. Similar results can be obtained for the MFPT averaged over the sphere volume $\langle t_2 \rangle$.

B. Comparison

Figure 2 shows that the coarse-grained approach and the exact solution are in good agreement for the values of the adsorption parameter $kR = 6.4 \cdot 10^{-4}$, $6.4 \cdot 10^{-3}$, $6.4 \cdot 10^{-2}$, which are used for an analogous plot in [23]. However, as soon as kR is large enough, the exact and approximate curves are significantly different, as illustrated on Fig. 3 (for $kR = 1$, 10, 100). Finally, and most importantly, the exact solution for the surface GMFPT $\langle t_1 \rangle$ can exhibit a minimum with respect to λ (see Fig. 3b) as opposed to the coarse-grained approach which always predicts a monotonic behavior. Similarly, the bulk GMFPT $\langle t_2 \rangle$ from Eq. (53) also exhibits a minimum with respect to λ for the parameters used in Fig. 3b (not shown).

Note that in all considered cases of Figs. 2, 3 the coarse-grained approach underestimates the search time at large λ. This discrepancy is due to the approximate expression of t_b used in [23] to estimate k_b. As expected, in a similar two-dimensional problem, our solution at large λ coincides with the earlier exact result of [24] for the mean exit time when the surface is perfectly reflecting (see Appendix E).

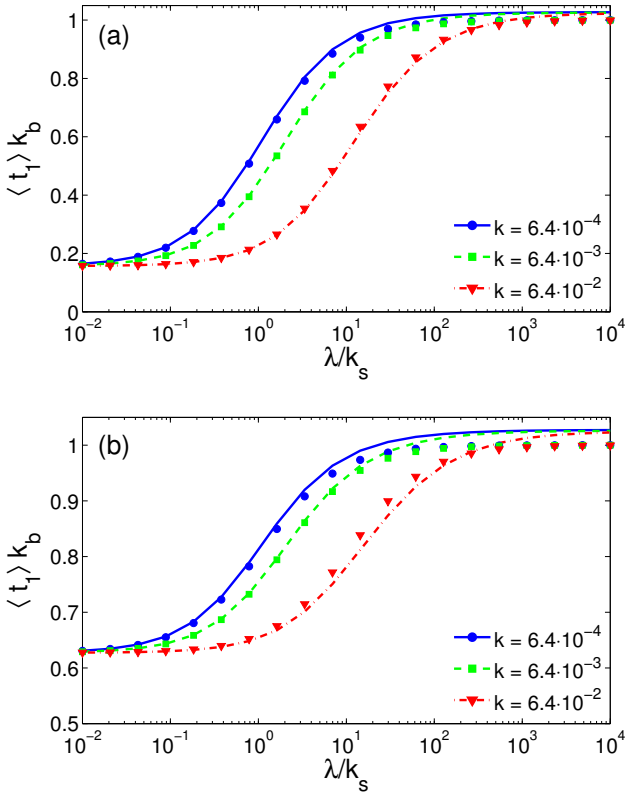

FIG. 2: (Color online) Comparison between the coarse-grained (symbols) and exact (lines) surface GMFPT $\langle t_1 \rangle$ as a function of the desorption rate λ, for $\epsilon = 0.02$, $N = 3 \cdot 10^4$ and several values of $kR = 6.4 \cdot 10^{-4},\ 6.4 \cdot 10^{-3},\ 6.4 \cdot 10^{-2}$ (from [23]), with $D_2 = D_1 = 1$ **(a)** and $D_2 = 4D_1 = 4$ **(b)** in arbitrary units in which $R = 1$.

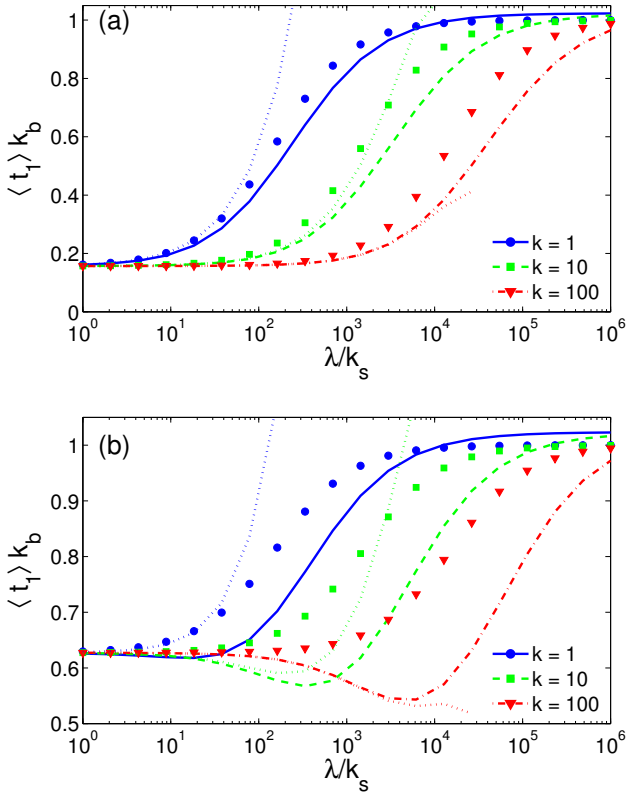

FIG. 3: (Color online). Comparison between the coarse-grained (symbols) and exact (lines) surface GMFPT $\langle t_1 \rangle$ as a function of the desorption rate λ, for $\epsilon = 0.02$, $N = 3 \cdot 10^4$ and several values of $kR = 1, 10, 100$, with $D_2 = D_1 = 1$ **(a)** and $D_2 = 4D_1 = 4$ **(b)**. The dotted curves illustrate the perturbative solution (62) which is accurate for moderate λ but strongly deviates for very large λ.

C. Discussion

We now discuss quantitatively the validity domain of the coarse-grained approach and explain qualitatively why it fails to reproduce the minimum of the surface GMFPTs with respect to λ.

As suggested in [23], the validity of the coarse-grained approach requires the equilibration times for homogenization within each state to be faster than the other time scales of the process. In particular, the equilibration rate should be larger than the following:
(i) the target encounter rate, i.e.,

$$\max(k_s, k_b) \ll \min(D_1/R^2, D_2/R^2), \qquad (66)$$

which implies $\epsilon \ll 1$. The coarse-grained approach can only describe narrow escape situations $\epsilon \ll 1$, as mentioned in [23], whereas the exact solution presented here is valid for arbitrary ϵ.
(ii) the inverse of the mean time for re-adsorption on the surface after desorption, i.e.,

$$\alpha = 3kD_2/R \ll \min(D_1/R^2, D_2/R^2), \qquad (67)$$

which implies in particular that $kR \ll 1$. Indeed, as seen in Appendix C, in the regime $kR \ll 1$, the spatial correlations between the starting and ending points of bulk excursions are negligible. The condition (67) is satisfied in the situations displayed in Fig. 2.

However, Eq. (67) is not longer satisfied in both situations of Fig. 3, and one notices that the coarse-grained solution does not match with the exact result. This is particularly visible in Fig. 3b, where the surface GMFPT $\langle t_1 \rangle$ exhibits a minimum with respect to the desorption rate λ.

The condition (67) for the applicability of the coarse-grained approach turns out to be incompatible with the existence of the minima of the bulk and surface GMFPTs with respect to λ. Such a minimum can be attributed to the fact that bulk excursions reduce the time loss due to the recurrence of surface Brownian motion by bringing the particle, through the bulk, to unvisited regions of the surface. In the coarse-grained approach, a bulk excursion $s \to b \to s$ "consumes" time but brings the particle back to its initial effective state s. The assumption that the starting and ending points of bulk excursions belong to

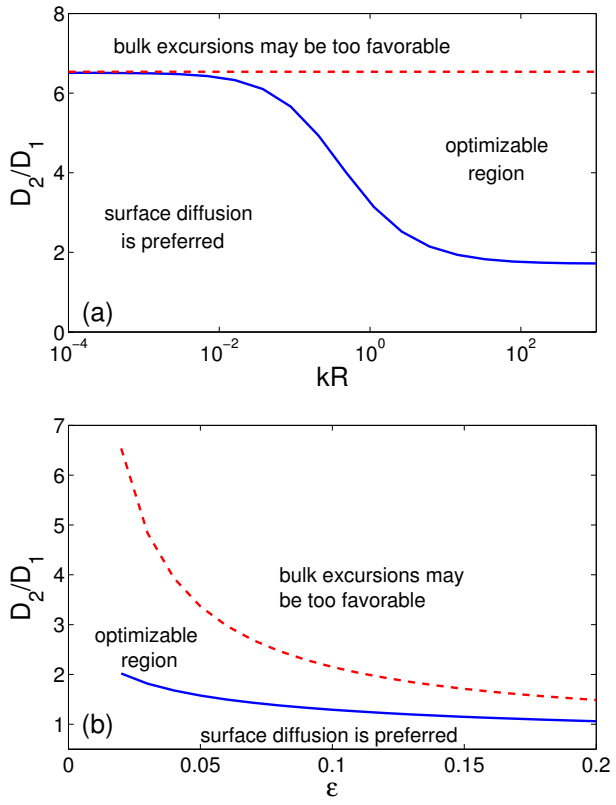

FIG. 4: (Color online). The regions of optimality for the surface GMFPT $\langle t_1 \rangle$. **(a)** The critical ratio D_2/D_1 as a function of the adsorption coefficient k for a fixed value of the target half-width $\epsilon = 0.02$; **(b)** The critical ratio D_2/D_1 as a function of the target size ϵ, for the adsorption coefficient $kR = 10$. Below the lower bound (dashed red line), surface diffusion is preferred. Above the upper bound (solid blue line), the GMFPT is smaller in the desorbed state than in the adsorbed state. In between, the surface GMFPT is an optimizable function of λ. Series are truncated at $N = 10^4$.

the same effective state s necessarily eludes the optimization property.

More precisely, bulk excursions are expected to be favorable if they are fast (e.g. large adsorption rate α) and long-ranged ($kR \ll 1$, see Appendix C). This is in clear contradiction with the condition (67) of applicability of the coarse-grained approach. Due to the relation $\alpha = 3kD_2/R$, this condition is achieved for a high enough diffusion coefficient D_2, which sets the lower bound of D_2/D_1 derived above. However, if the ratio D_2/D_1 is too large, bulk excursions can be too favorable so that the optimum would be achieved for $\lambda = \infty$. The upper bound $(D_2/D_1)_{\rm up}$ in Eq. (60) excludes this possibility. The set of conditions on the diffusion coefficients ratio is illustrated on Fig. 4.

Understanding by analytical means the agreement between the exact and coarse-grained expressions of Eqs. (49) and (65) under the assumptions of Eqs. (66) and (67) is a challenging question. A first step in this direction is presented in Appendix B, in which the agreement is found within the domain of applicability of the perturbative expansion (introduced in Sec. III E).

V. CONCLUSION

We have obtained an exact expression for the MFPT and their spatial averages, called bulk and surface GMFPTs, for the process studied in [23]. Compared to [12, 13], the introduction of the surface binding rate k allowed one to avoid using the ejection distance a (i.e. to set $a = 0$) after each desorption events. In contrast to the statement of [23], we have shown that the bulk and surface GMFPTs can be optimized even in this situation and that this optimality property is not related to the non-locality of the intermittent process considered in [12, 13].

These exact results can be extended in several directions to include the following: (i) the search for a semi-reflecting target, with an adsorption parameter different from the rest of the surface (see Appendix D); (ii) the 2D search for an angular aperture on the boundary of a disk (see Appendix E); and (iii) the biased search for an arbitrary number of regularly spaced targets over an otherwise semi-reflecting annulus (2D) or cone (3D), following the method of [22]. Notably, even for a 3D search for a purely reflecting target and for a 2D search with a bulk diffusion coefficient D_2 smaller than the surface diffusion coefficient D_1, the surface GMFPT can be an optimizable function with respect to the desorption rate (see Figs. 6 and 7 below).

Acknowledgments

O.B. is supported by the ERC Starting Grant No. FPTOpt-277998.

Appendix A: Boundary condition on the MFPT

The diffusion equation and the boundary condition for the occupation probability distribution in the bulk appear at first sight to be different in [23] and [22]. In this section, we show that these two sets of equations are in agreement and lead to the same radiative boundary condition (15) for the MFPT.

In [22] we defined a different set of equations for the conditional probability distribution to include a radial ejection distance a after each desorption event, in the presence of a velocity field. With the shorthand notations of Sec. III A, the forward advection-diffusion equation of

[22] reads:

$$\frac{\partial p(r,\theta)}{\partial r}_{|R} = -\,k\,p(R,\theta) + \frac{v(R)}{D_2}p(R,\theta), \tag{A1}$$

$$\frac{\partial p(r,\theta)}{\partial s} = D_2\,\left(\Delta_{(r,\theta)} + \frac{v(r)}{D_2 r}\right)\,p(r,\theta) + \lambda\,\left(\frac{R}{R-a}\right)^2\,\delta^3(\mathbf{r}-(R-a,\theta))\,p(\theta), \tag{A2}$$

where $v(r)$ is a radial velocity field positive for an outward drift. The other diffusion equations on the conditional probabilities are the same as in [22].

Notice that Eq. (A1) does not involve the desorption rate λ. However there is no contradiction with Eq. (16), as Eq. (A1) (without drift) leads the same backward boundary Eq. (19) as long the appropriate limit for $a = 0$ in the Dirac function in Eq. (A2) is

$$\int_0^R \left(\frac{R}{R-a}\right)^2 \delta(r-(R-a,\theta))p(r,\theta)r^2 dr \xrightarrow{a\to 0} R^2 p(R,\theta),$$

It can be proved that this condition is required from normalization of the probability density.

Appendix B: Analytical agreement between the coarse-grained and exact solutions

Figure 2 shows a good agreement between the exact and coarse-grained expressions (49, 65). However, finding an explicit analytical relation between these two expressions under the general conditions (66, 67) seems nontrivial.

We focus here on the following specific successive limits: (i) small target extension ($\epsilon \ll 1$); (ii) low-desorption rate regime ($\lambda \ll k_s$); (iii) and intermediate range for the adsorption rate: $k_b \ll \alpha \ll \min(D_2/R^2, D_1/R^2)$.

On one hand, the coarse-grained expression in these limits reads

$$\langle t_1\rangle \approx \left(1+\frac{\lambda}{\alpha}\right)t_s + O\left(\epsilon, \frac{\lambda}{k_s}\right), \tag{B1}$$

where we have used that $k_b/k_s \ll 1$ and $k_b/\alpha \ll 1$ for a fixed value of α at sufficiently small $\epsilon \ll 1$.

On the other hand, in the limit $\epsilon \ll 1$ the perturbative expansion of Eq. (62) is accurate. In the abovementionned limits it reads

$$\langle t_1\rangle \approx \left(1+\frac{\lambda}{\alpha}\right)t_s + O(\epsilon, \lambda/k_s, kR), \tag{B2}$$

where we have used that

$$\sum_{n=1}^{\infty} \frac{2n+1}{n(n+1)}\,\frac{\frac{n}{kR}}{n(n+1)(1+\frac{n}{kR})+\frac{\lambda R^2}{D_1}\frac{n}{kR}} \approx 1 + O(kR, R^2\lambda/D_1), \tag{B3}$$

and that the condition $R^2\lambda/D_1 \ll 1$ is guaranteed from the condition $\lambda/k_s \ll 1$.

The identification of the first order terms in Eqs. (B1, B2) shows analytically the agreement between the coarse-grained and exact solutions within a range of parameters which necessarily satisfies Eqs. (66, 67). Notice that the argument presented here relies on the condition $k_b/\alpha \ll 1$ which is not satisfied in the situations represented on Fig. 2.

Appendix C: Measure of correlations

In this section we quantify the spatial correlations between the starting and ending points of a bulk excursion. We then provide the range of values for k in which the spatial correlations are negligible. The probability density $\Pi(\theta)$ for a particle initially started from the surface state at the angle $\theta_0 = 0,\ \phi_0 = 0$ to first return on the surface to any point (θ, ϕ) (with $\phi \in [0, 2\pi]$) is [22]

$$\Pi(\theta) = \frac{\sin\theta}{2}\left(1 + \sum_{n=1}^{\infty}\frac{2n+1}{1+\frac{n}{kR}}P_n(\cos\theta)\right). \tag{C1}$$

The cumulative probability distribution for the relocation angle $\theta \in [0,\pi]$ is the integral of the probability density

$$F(\theta) \equiv \frac{1}{2}\int_{-\pi}^{\theta} \Pi(\theta')\sin\theta'\ d\theta'. \tag{C2}$$

By analogy with the Kolmogorov-Smirnov test [25], we propose to measure the spatial correlations between the starting and ending points of a bulk excursion by the norm

$$N_K \equiv \max_{\theta\in[0,\pi]} |\delta F(\theta)|\,, \tag{C3}$$

with

$$\delta F(\theta) \equiv F(\theta) - F_u(\theta) = \frac{1}{2}\sum_{n=1}^{\infty}\frac{P_{n-1}(\cos\theta) - P_{n+1}(\cos\theta)}{1+\frac{n}{kR}}, \tag{C4}$$

and $F_u(\theta) = (1-\cos\theta)/2$ is the cumulative distribution for uncorrelated random relocation on the sphere. This leads a correlation angle Θ which is defined as the solution of the equation $\delta F(\Theta) = N_K$.

As shown on Fig. 5, the spatial correlation is negligible ($N_K \ll 1, \Theta \approx 1$) as long as $kR < 1$. In particular for the reference values $kR = 6.4\cdot 10^{-4},\ 6.4\cdot 10^{-3},\ 6.4\cdot 10^{-2}$ used in [23], the norm N_K is smaller than 0.05 and the correlation length is nearly constant at $\Theta \approx 1.2$.

Appendix D: Generalization to semi-reflecting targets

In this section, we briefly generalize our method to the case of a semi-reflecting target, for which the B.C. reads

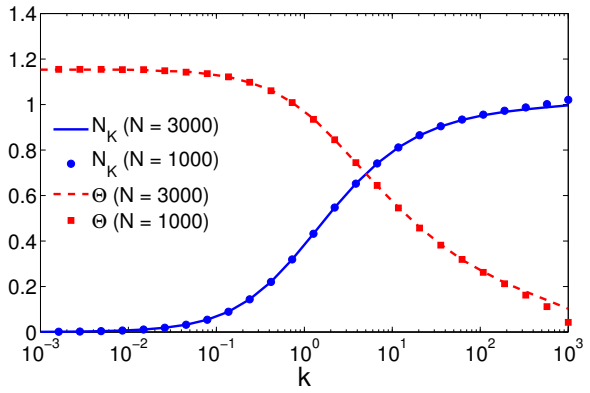

FIG. 5: (Color online). The norm N_K (blue solid line and circles) and the correlation angle Θ in radians (red dashed line and squares) as functions of the adsorption coefficient k, for the truncation size $N = 3000$ (lines) and $N = 1000$ (symbols).

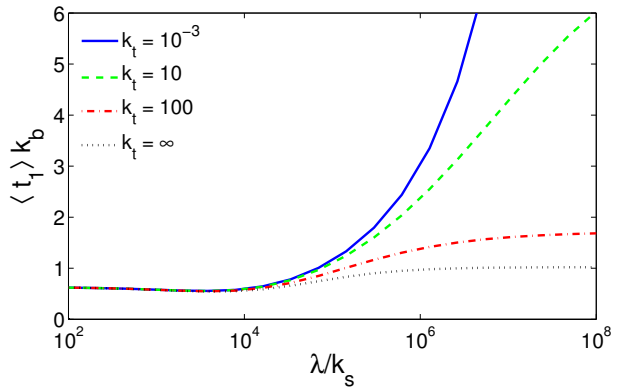

FIG. 6: (Color online). The surface GMFPT $\langle t_1 \rangle$ as a function of the desorption rate λ, for several values of the target adsorption parameter k_t (for particles hitting the target from the bulk), with $\epsilon = 0.02$ and $D_2 = D_1 = 1$ in units in which $R = 1$. The non-reactive part of the surface is semi-reflecting with an adsorption parameter $k = 100$. Note that the target is perfectly reactive for particles adsorbed on the surface. Series are truncated at $N = 3 \cdot 10^4$.

as

$$t_2(R,\theta) = \begin{cases} -\dfrac{1}{k_t}\dfrac{\partial t_2}{\partial r}_{|\mathbf{r}=(R,\theta)} & (0 \le \theta \le \epsilon), \\ t_1(\theta) - \dfrac{1}{k}\dfrac{\partial t_2}{\partial r}_{|\mathbf{r}=(R,\theta)} & (\epsilon < \theta \le \pi). \end{cases} \quad \text{(D1)}$$

This general description includes the following cases:

- $k_t = \infty$ is the case considered so far in the present article of a fully adsorbing target, Eq. (15);
- $k_t = k$ is considered in Ref. [22];
- $k_t = 0$ corresponds to a target which is fully reflecting for particles hitting the target from the bulk.

Using the mixed boundary condition (D1), the projection of a series representation (23) for $t_2(R,\theta)$ onto the basis $\{V_n(\theta)\}_{n\ge 0}$ becomes

$$\int_0^\pi \left(t_2(R,\theta) + \frac{1}{k_t}\frac{\partial t_2}{\partial r}_{|\mathbf{r}=(R,\theta)} \right) V_n(\theta) d\mu(\theta) = \quad \text{(D2)}$$
$$\int_\epsilon^\pi t_1(\theta) V_n(\theta) d\mu(\theta) - \int_\epsilon^\pi \left(\frac{1}{k} - \frac{1}{k_t} \right) \frac{\partial t_2}{\partial r}_{|R} V_n(\theta) d\mu(\theta),$$

which replaces Eq. (24), with $d\mu(\theta) = \frac{1}{2}\sin\theta d\theta$. This leads to the following equations on coefficients α_n:

$$\alpha_0 = \langle t_1 | 1 \rangle - \frac{R^2}{2dD_2}\left(1 + 2\left(\frac{1}{kR} - \frac{1}{k_t R}\right) K_{00}^{(\epsilon)}\right) - \sum_{m=1}^{\infty} m \left(\frac{1}{kR} - \frac{1}{k_t R}\right) K_{0m}^{(\epsilon)}\, \alpha_m, \quad \text{(D3)}$$

$$\alpha_n \left(1 + \frac{n}{k_t R}\right) = \langle t_1 | V_n \rangle + \frac{R^2}{dD_2}\left(\frac{1}{kR} - \frac{1}{k_t R}\right) K_{n0}^{(\epsilon)} - \sum_{m=1}^{\infty} m \left(\frac{1}{kR} - \frac{1}{k_t R}\right) K_{nm}^{(\epsilon)}\, \alpha_m \quad (n \ge 1). \quad \text{(D4)}$$

From these equations, we extend the definition of M_{nm} and $\hat{U}_m$ from Eq. (28) to

$$M_{nm} \equiv \delta_{mn}\frac{n}{k_t R} + m\left(\frac{1}{kR} - \frac{1}{k_t R}\right) K_{nm}^{(\epsilon)}, \quad \text{(D5)}$$

$$\hat{U}_n \equiv \langle t_1 | V_n \rangle + \frac{R^2}{dD_2}\left(\frac{1}{kR} - \frac{1}{k_t R}\right) K_{n0}^{(\epsilon)}. \quad \text{(D6)}$$

Following the same steps as in Sec. III B, one gets an integral equation on the dimensionless MFPT $\psi(\theta)$:

$$\psi(\theta) = g_\epsilon(\theta) + \sum_{n,m=1}^{\infty} \frac{V_n(\theta) - V_n(\epsilon)}{\rho_n} X_{nm} \quad \text{(D7)}$$
$$\times \left(\frac{R^2}{dD_2 T}\left(\frac{1}{kR} - \frac{1}{k_t R}\right) K_{0m}^{(\epsilon)} + \omega^2 \langle \psi | V_m \rangle \right),$$

which generalizes Eq. (39). Expanding this function onto the basis $\{V_n(\theta) - V_n(\epsilon)\}$ yields Eq. (47), with

$$U_n \equiv \frac{1}{\rho_n} \sum_{m=1}^{\infty} X_{nm} \left(\frac{\xi_m}{\rho_m} + \frac{R^2}{dD_2} \left(\frac{1}{kR} - \frac{1}{k_t R} \right) \frac{K_{m0}^{(\epsilon)}}{\omega^2 T} \right), \tag{D8}$$

which generalizes Eq. (43). This relation can also be written as

$$U_n = Z_n + \frac{D_1}{dD_2(1+\lambda/\alpha)} \left(\frac{1}{kR} - \frac{1}{k_t R} \right) W_n, \tag{D9}$$

where Z_n and W_n are still defined through Eqs. (55, 56). Other quantities and representations remain unchanged. Repeating the computation of the derivative of $\langle t_1 \rangle$ at $\lambda = 0$, one gets the lower bound as

$$\left(\frac{D_2}{D_1} \right)_{\text{low}} = -\frac{1}{dkR} \frac{\langle g_\epsilon \rangle + (\boldsymbol{\xi} \cdot \boldsymbol{W})(1 - k/k_t)}{(\boldsymbol{\xi} \cdot \boldsymbol{Z})}. \tag{D10}$$

which extends Eq. (58).

One can see that the change in the boundary condition, i.e., extension from Eq. (15) to Eq. (D1), does not affect the method and the structure of the solution. As a consequence, the conclusions on the optimility of the surface GMFPT remain qualitatively unchanged, although values of the lower bound may be different. Note that the determination of the upper bound requires the expression of the surface GMFPT for a semi-reflecting target in an otherwise reflecting sphere, which is still unknown.

As shown on Fig. 6, optimization in λ remains possible even in the case of a target which is fully reflecting for particles hitting the target from the bulk.

Appendix E: Application to a disk

$V_n(\theta)$	$\sqrt{2}\cos(n\theta)$
$g_\epsilon(\theta)$	$\frac{1}{2}(\theta-\epsilon)(2\pi-\epsilon-\theta)$
$\langle g_\epsilon \vert 1 \rangle_\epsilon \equiv \langle g_\epsilon \rangle_\epsilon$	$\frac{1}{3\pi}(\pi-\epsilon)^3$
$\xi_n \ (n \geq 1)$	$-\frac{\sqrt{2}}{\pi}\{(\pi-\epsilon)\cos(n\epsilon) + \sin(n\epsilon)/n\}$
$K_{00}^{(\epsilon)}$	$(\pi-\epsilon)/\pi$
$K_{n0}^{(\epsilon)} \quad (n \geq 1)$	$-\frac{\sqrt{2}}{n\pi}\sin(n\epsilon)$
$K_{nn}^{(\epsilon)} \quad (n \geq 1)$	$\frac{1}{\pi}\left(\pi - \epsilon - \frac{\sin(2n\epsilon)}{2n}\right)$
$K_{nm}^{(\epsilon)} \quad n,m \geq 1, m \neq n$	$\frac{1}{\pi}\left(\frac{\sin((m-n)\epsilon)}{m-n} + \frac{\sin((m+n)\epsilon)}{m+n}\right)$
$I_{nn}^{(\epsilon)} \ (n \geq 1)$	$\frac{1}{\pi}\left(\pi - \epsilon + \frac{\sin 2n\epsilon}{2n}\right)$
$I_{nm}^{(\epsilon)} \quad m,n \geq 1, m \neq n$	$\frac{2}{\pi}\frac{\cos(n\epsilon)\frac{\sin(m\epsilon)}{m} - \cos(m\epsilon)\frac{\sin(n\epsilon)}{n}}{n^2-m^2} \ m^2$

TABLE II: Summary for the 2D case of the quantities involved in the computation of the vector $\boldsymbol{\xi}$ and the matrices Q and M in Eqs. (43, 45) that determine the Fourier coefficients d_n of $t_1(\theta)$ according to Eq. (47).

In 2D, the diffusion equations on the MFPT are identical to Eqs. (12, 13) provided the change of definition for the Laplace operators:

$$\Delta_r = \frac{\partial^2}{\partial r^2} + \frac{1}{r}\frac{\partial}{\partial r}, \qquad \Delta_\theta = \partial_\theta^2.$$

The eigenfunctions $V_n(\theta)$ and eigenvalues ρ_n of the angular Laplace operator Δ_θ become

$$V_n(\theta) = \sqrt{2}\cos n\theta, \qquad \rho_n = n^2 \qquad (n \geq 0). \tag{E1}$$

The inner scalar product (21) is replaced by

$$(f,g) \to \langle f|g \rangle_\epsilon \equiv \frac{1}{\pi}\int_\epsilon^\pi f(\theta)g(\theta)d\theta. \tag{E2}$$

In Table II, we summarize the expressions for the matrix elements $K_{mn}^{(\epsilon)}$ and $I_{mn}^{(\epsilon)}$ which replace those from Table I. One has also to replace Eq. (37) by

$$g_\epsilon(\theta) = \frac{1}{2}(\theta-\epsilon)(2\pi-\epsilon-\theta). \tag{E3}$$

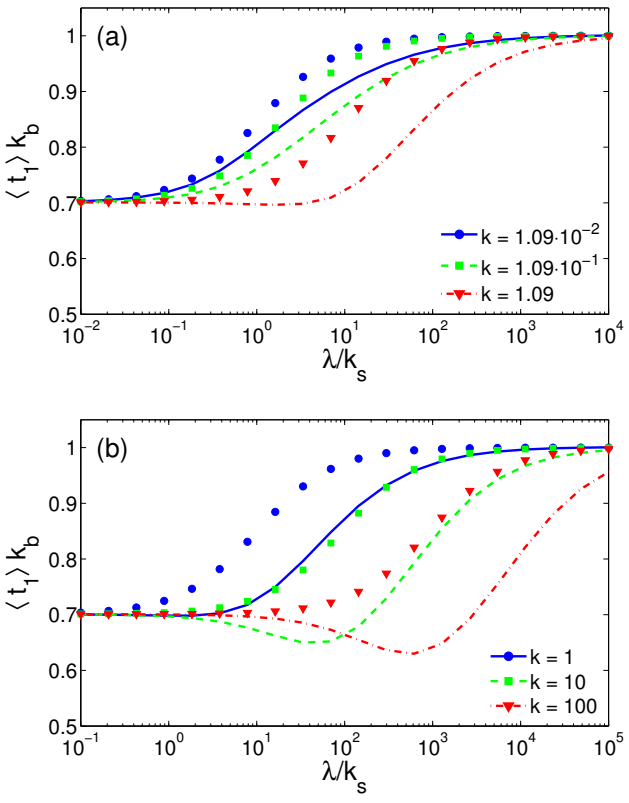

FIG. 7: (Color online). The surface GMFPT $\langle t_1 \rangle$ in the disk as a function of the desorption rate λ, for $\epsilon = 0.02$, $D_2/D_1 = 1$, and **(a)** $kR = 1.09 \cdot 10^{-2}$, $1.09 \cdot 10^{-1}$, 1.09 (corresponding to $\alpha = 0.1k_b, k_b, 10k_b$) and **(b)** $kR = 1,\ 10,\ 100$. Series are truncated at $N = 3 \cdot 10^4$.

The method of derivation and the remaining quantities are not modified. In particular, Eq. (48) for the MFPT $t_1(\theta)$, Eq. (49) for the surface GMFPT $\langle t_1 \rangle$ and

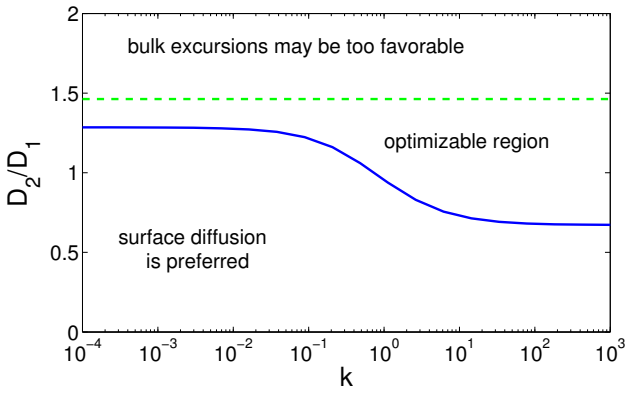

FIG. 8: (Color online). The regions of optimality for the surface GMFPT $\langle t_1 \rangle$ for a disk of radius $R = 1$ with an aperture of half-width $\epsilon = 0.02$. Below the lower bound (solid red line) surface diffusion is preferred. Above the upper bound (dashed green line), the surface GMFPT is higher in the adsorbed state than in the desorbed state. In between, the surface GMFPT is an optimizable function of λ. Series are truncated at $N = 10^4$.

Eq. (58) for the lower bound on the diffusion coefficient ratio $(D_2/D_1)_{\rm low}$ are applicable for the disk. In turn, the asymptotic relations on the exit time (2, 3) are modified:

$$t_s = \langle t_1 \rangle_{\lambda=0} = \frac{R^2}{D_1} \, \frac{(\pi - \epsilon)^3}{3\pi}, \qquad \text{(E4)}$$

$$t_b = \langle t_1 \rangle_{\lambda \to \infty} \simeq \frac{R^2}{D_2} \left[\ln(2/\epsilon) + O(1) \right] \qquad \text{(E5)}$$

that leads to the following expression for the upper bound on the diffusion coefficients

$$\left(\frac{D_2}{D_1} \right)_{\rm up} = \frac{3\pi \ln(2/\epsilon)}{(\pi - \epsilon)^3} + O(1). \qquad \text{(E6)}$$

Figure 7 illustrates the fact that the surface GMFPT is an optimizable function of the desorption rate λ in the range of parameters represented on Fig. 8.

[1] R. Walder, N. Nelson, and D. K. Schwartz, Physical Review Letters **107**, 156102 (2011).
[2] A. V. Chechkin, I. M. Zaid, M. A. Lomholt, I. M. Sokolov, and R. Metzler, Physical Review E **79** (2009).
[3] Z. Schuss, A. Singer, and D. Holcman, Proceedings of the National Academy of Sciences **104**, 16098 (2007).
[4] B. Alberts, A. Johnson, J. Lewis, M. Raff, K. Roberts, and P. Walter, *Molecular Biology of the Cell* (Garland New York, 2002).
[5] O. V. Bychuk and B. O'Shaughnessy, Physical Review Letters **74** (1995).
[6] G. C. Bond, *Heterogeneous Catalysis: Principles and Applications* (Clarendon, Oxford, 1987).
[7] R. D. Astumian and P. B. Chock, The Journal of Physical Chemistry **89**, 3477 (1985).
[8] O. G. Berg, R. B. Winter, and P. H. von Hippel, Biochemistry **20**, 6929 (1981).
[9] H. Sano and M. Tachiya, The Journal of Chemical Physics **75**, 2870 (1981).
[10] G. Adam and M. Delbrück, *Reduction of dimensionality in biological diffusion processes* (W.H. Freeman Co, Publishers, San Francicso, 1968).
[11] O. Bénichou, C. Loverdo, M. Moreau, and R. Voituriez, Reviews of Modern Physics **83** (2011).
[12] O. Bénichou, D. Grebenkov, P. Levitz, C. Loverdo, and R. Voituriez, Journal of Statistical Physics **142**, 657 (2011).
[13] O. Bénichou, D. Grebenkov, P. Levitz, C. Loverdo, and R. Voituriez, Physical Review Letters **105**, 150606 (2010).
[14] T. Calandre, O. Bénichou, D. S. Grebenkov, and R. Voituriez, Physical Review E **85**, 051111 (2012).
[15] Z. Schuss, Journal of Scientific Computing pp. 1–17 (2012).
[16] S. Pillay, M. Ward, A. Peirce, and T. Kolokolnikov, Multiscale Modeling and Simulation **8**, 803 (2010).
[17] C. Chevalier, O. Bénichou, B. Meyer, and R. Voituriez, Journal of Physics A: Mathematical and Theoretical **44**, 25002 (2011).
[18] I. V. Grigoriev, Y. A. Makhnovskii, A. M. Berezhkovskii, and V. Y. Zitserman, The Journal of Chemical Physics **116**, 9574 (2002).
[19] F. Rojo and C. E. Budde, Physical Review E **84**, 21117 (2011).
[20] F. Rojo, H. S. Wio, and C. E. Budde (2012), arXiv:1206.2204v1.
[21] G. Oshanin, M. Tamm, and O. Vasilyev, The Journal of Chemical Physics **132**, 235101 (2010).
[22] J. F. Rupprecht, O. Bénichou, D. Grebenkov, and R. Voituriez, Journal of Statistical Physics **147**, 891 (2012).
[23] A. M. Berezhkovskii and A. V. Barzykin, The Journal of Chemical Physics **136**, 54115 (2012).
[24] A. Singer, Z. Schuss, and D. Holcman, Journal of Statistical Physics **122**, 465 (2006).
[25] J. Massey, J. Franck,, Journal of the American Statistical Association **46**, pp. 68 (1951).
[26] J.J. Linderman, D.A. Lauffenburger, Biophysical Journal **50**, pp. 295 (1986).
[27] C. Gardiner, *Handbook of Stochastic Methods for Physics, Chemistry and Natural Sciences* (Springer, 2004).
[28] S. Redner, *A guide to First- Passage Processes* (Cambridge University Press, Cambridge, England, 2001).